The Influence of Environment on Solar Chimney Power Plant Performance

JP Pretorius[a] and DG Kröger[b]
Received 4 December 2008 and accepted 25 September 2009

This paper investigates the effects of ambient wind, temperature lapse rates and nocturnal temperature inversions on the performance of a large-scale solar chimney power plant. The effect of prevailing ambient winds at a reference site on plant performance is evaluated, while different ambient wind profile models are also considered. During the daytime, the atmosphere surrounding the plant is modelled using a dry adiabatic lapse rate (DALR) and the International Standard Atmosphere (ISA), while night-time temperature inversion effects are also accounted for. Results indicate that windy conditions impair plant performance considerably, while nocturnal temperature inversions cause significant reductions in night-time output.

Nomenclature

b	Exponent
c	Specific heat capacity [J/kgK]
C	Coefficient
d	Diameter [m]
e	Emissivity
g	Gravitational acceleration [9.8 m/s^2]
H	Height [m]
k	Thermal conductivity [W/mK]
K	Loss coefficient
n	Refractive index or number or exponent
p	Pressure [N/m^2]
P	Pitch [m]
r	Radius [m]
R	Gas constant
t	Thickness [m] or time after sunset [hours]
T	Temperature [K or °C]
z	Height above ground or sea level [m]

Greek symbols

α	Absorptivity
Δ	Differential
ε	Roughness [m]
η	Efficiency [%]
ρ	Density [kg/m^3]

Subscripts

a	Ambient air
bw	Bracing wheel
c	Chimney
co	Chimney outlet
d	Day
e	Extinction
g	Ground
i	Inlet
int	Intersection
max	Maximum
r	Roof or radial
ref	Reference
s	Support
sD	Support drag
sl	Sea level
t	Tangential
tg	Turbo-generator
turb,i	Turbine inlet
w	Wind

a, b Department of Mechanical and Mechatronic Engineering University of Stellenbosch
Private Bag X1, Matieland, 7602.
E-mail: jp.pretorius@eskom.co.za

1. Introduction

A solar chimney power plant consists of a translucent circular canopy or roof raised a certain height above the ground, with a chimney or circular tower at its centre (figure 1). The chimney houses one or more turbines at its base, (each) connected to an electric generator. Solar radiation penetrates the collector roof and heats the ground surface beneath, which in turn heats the adjacent air. The warm air under the roof flows towards and up into the chimney. The air flowing through the chimney drives the turbo-generator(s), which subsequently generates electricity.

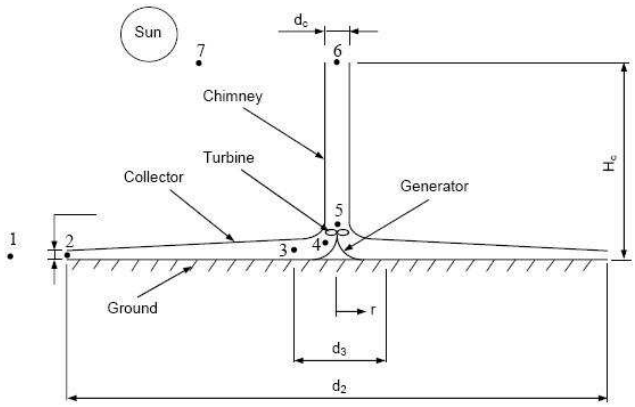

Figure 1: Schematic illustration of a solar chimney power plant

2. Literature Review

Haaf *et al.*[1] discuss the basic principles behind the operation, construction and power generation of a solar chimney power plant, while Haaf [2] presents preliminary test results from a prototype plant built in Manzanares, Spain in 1982. Schlaich[3] endorses the use of solar chimney power plants for future electricity generation and also communicates details of the construction, materials, operation, tests and experimental data of the pilot solar chimney plant in Manzanares. Pasumarthi and Sherif[4] published an approximate mathematical model for a solar

chimney, followed by a subsequent article (Pasumarthi and Sherif [5]) which validates the model against experimental results from the pilot plant. Kröger and Buys[6] and Gannon and Von Backström[7] perform early comprehensive analyses on the performance of solar chimney power plants, while Gannon and Von Backström[8] also conduct a study concerning solar chimney turbine performance. An analytical and numerical model is developed by Bernardes *et al.*[9], presenting a comparison between simulated results and experimental measurements from the pilot plant at Manzanares. Pastohr *et al.*[10] conduct a basic temperature and flow field analysis using a numerical CFD package and compare their results to another simple numerical model. A relatively detailed numerical model is developed by Pretorius *et al.*[11], simulating the performance of a large-scale reference solar chimney power plant. A publication by Serag-Eldin[12] conducts a simple study into the effect of atmospheric winds on the flow patterns under the collector roof of a small-scale solar chimney power plant. A mathematical model is developed by Bilgen and Rheault[13] for evaluating the performance of solar chimney power plants at high latitudes. A refined numerical model for simulating large solar chimney plants is presented by Pretorius and Kröger[14], while Pretorius and Kröger[15] also conduct a sensitivity analysis on the operating and technical specifications of a solar chimney power plant.

The current paper employs the exact numerical model and specified reference plant (see appendix of this paper) as presented by Pretorius and Kröger[14].

3. Wind Effects

Ambient winds affect the operation of a solar chimney power plant in a number of ways. Convection losses from the collector roof to the environment are increased as cross-winds blow over the roof. The air-flow through the plant is also altered by winds blowing across the chimney outlet. In addition, ambient cross-winds which blow in under the collector roof also affect the air-flow through the plant.

The numerical model of the present study only considers the effect of prevailing winds on top of the collector roof surface and at the top of the chimney, while neglecting any flow pattern distortions under the collector roof as a result of ambient winds.

The chosen location of the reference solar chimney power plant is near Sishen, South Africa (see appendix). The prevailing ambient wind speeds at this location are presented by Pretorius and Kröger[14] and are those wind speeds measured at 10 m above ground level.

3.1 Wind profiles

This subsection evaluates the effect of three different wind profiles on the performance of a solar chimney power plant. It should be noted that the numerical model assumes that the wind speed over the entire top collector roof surface is equal to the particular wind speed at 10 m above ground level at that specific time. The publication by Pretorius and Kröger[14] discusses how ambient cross-winds at the chimney outlet are modelled by the numerical simulation model.

3.1.1 Simulation and results

Comparative simulations are performed for the reference solar chimney power plant (see appendix), with two of the models incorporating the following well-known power-law profile

$$\frac{v_w}{v_{w,ref}} = \left(\frac{z}{z_{ref}} \right)^{1/n} \quad (1)$$

where v_w is the wind velocity at a specific height z above ground level, $v_{w,ref}$ is the wind velocity at a reference height above ground level z_{ref} and n is the power-law exponent. These two models employ respective exponents of $n = 5$ and $n = 7$ for the power-law wind profile. Another model assumes a linear wind profile, approximating the ambient wind speed at the chimney outlet as twice the value at 10 m above ground level. Simulations are repeated for chimney heights of H_c = 500 m, 1000 m and 1500 m.

The authors realize that no standard wind profile exists and that the fluid dynamic analysis of the earth's boundary layer is an extremely complex exercise. Previous simple attempts at modelling the atmospheric boundary layer have yielded the power-law profile of equation 1. It is not the aim of this analysis to model wind profiles accurately, but instead to present trends of solar chimney power plant performance in the presence of ambient winds. It should also be noted that the effects of cold inflow are neglected in the analysis of this section.

Figures 2, 3 and 4 depict the three mentioned wind profile approximations for chimney heights of H_c = 500 m, 1000 m and 1500 m respectively. For purposes of illustration, a typical wind speed of v_w = 2 m/s is chosen at 10 m above ground level. It is clear that all the profiles employ equal wind velocities at 10 m above ground level, while differing wind velocities are predicted at the chimney outlet height.

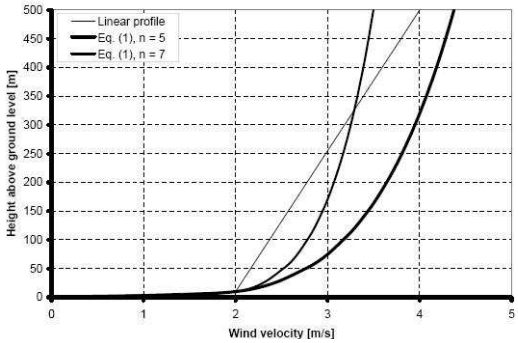

Figure 2: The linear and power-law wind profiles for a 500 m high chimney (v_w = 2 m/s at 10 m above ground level)

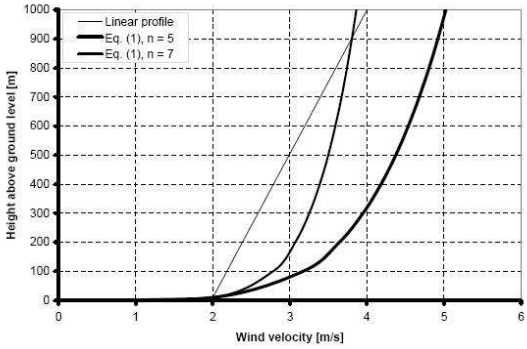

Figure 3: The linear and power-law wind profiles for a 1000 m high chimney (v_w = 2 m/s at 10m above ground level)

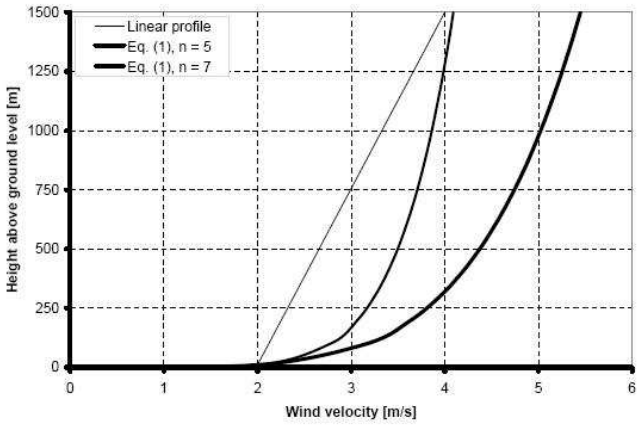

Figure 4: The linear and power-law wind profiles for a 1500 m high chimney (v_w = 2 m/s at 10 m above ground level)

Table 1 illustrates the insignificant difference in annual output between the models employing the various approximated wind profiles.

Chimney height [m]	Wind profile	Annual power output [GWh]
500	Linear	159.2
	equation 1, n = 5	164.5
	equation 1, n = 7	157
1000	Linear	336
	equation 1, n = 5	343.6
	equation 1, n = 7	335.6
1500	Linear	521.1
	equation 1, n = 5	528.5
	equation 1, n = 7	521.5

Table 1: Annual solar chimney power plant performance for various wind profile approximations

In addition, when comparing table 1 and figures 2, 3 and 4 it is evident that in each case the plant model that employs the wind profile which predicts the greatest wind velocity at the height of the chimney outlet also predicts the highest annual power output. For example, consider figure 2. The power-law wind profile with n = 5 predicts the greatest wind velocity at a chimney height of 500 m. Now consider table 1, where for a chimney height of H_c = 500 m the plant model employing the power-law profile with n = 5 gives the highest annual power output (compared to the other models with H_c = 500 m). The plant model employing the wind profile which predicts the second highest wind velocity at the chimney outlet height also predicts the second highest annual power output, etc. Similar findings are presented for H_c = 1000 m and H_c = 1500 m.

An in-depth evaluation of the simulation data reveals the following. All of the above-mentioned plant models experience periods in the winter months where the ambient winds generate a suction effect of air through the chimney, which is ultimately responsible for a slightly enhanced power production. This is caused due to a pressure rise (Δp_{co}) at the chimney outlet, as discussed by Pretorius and Kröger[14] (specifically, equations 48, 51 and 52). During the winter months (mostly during night-time) the driving potential of the plant is relatively low and thus more sensitive to suction due to wind. During the summer months the driving potential is much greater, causing the suction effect to have a negligible influence on plant performance.

Therefore, the plants modelling the highest wind velocity at the chimney outlet also predicts the greatest annual power output as a result of predicting the greatest suction effect.

3.2 Influence of wind on plant performance

3.2.1 Simulation and results

Comparative computer simulations were run for the reference solar chimney power plant. Figure 5 compares the power output curves of the reference plant model (which includes windy ambient conditions) with that of the reference plant model which assumes quiet ambient conditions (no wind). It should be noted that the numerical model employs the linear wind profile mentioned in the previous subsection.

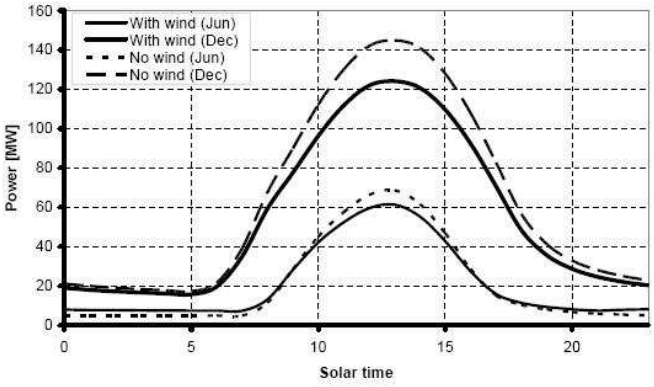

Figure 5: Effect of ambient wind on plant power output

From figure 5 it is clear that the prevailing winds significantly decrease the plant power output. This is primarily due to the convective heat losses from the collector roof to the environment. Notwithstanding higher suction effects at the chimney outlet which would cause greater power production, the windy conditions result in an increased convective heat transfer coefficient, facilitating a greater heat flux from the collector roof to the environment and ultimately lower power output. This convection heat transfer coefficient is evaluated according to equations 11 and 12 of Pretorius and Kröger[14].

When regarding figure 5 more closely, one finds that during the mornings and evenings of June (winter), the plant generates a slightly higher power output during windy conditions than during no-wind conditions. Two factors contribute to this phenomenon. Firstly, the ambient temperatures at these times are marginally higher than the

corresponding collector roof temperatures. Therefore, the windy conditions actually cause a minor convective heat flux from the environment to the collector roof, resulting in a slightly increased plant power output. Secondly, as mentioned in the previous subsection, a slight suction effect due to ambient winds is experienced at the top of the chimney during these times, which boosts the power output somewhat.

We can also further analyze the influence of ambient winds by regarding its effect on the annual power output of the solar chimney power plant. Table 2 gives an annual power output comparison of the two models which were simulated.

Plant configuration	Annual power output [GWh]
Windy ambient conditions	336
Quiet ambient conditions	373.2

Table 2: Annual power output comparison, illustrating the effect of ambient winds on solar chimney power plant performance

From table 2 it is clear that if the quiet ambient conditions are assumed at the proposed site, the annual power output of the plant increases by approximately 11.1 %.

4. Ambient Temperature Lapse Rate Effects

The reference plant of this paper assumes a dry adiabatic lapse rate (DALR) for the air inside the chimney and the atmosphere surrounding the solar chimney power plant. These are believed to be good approximations of the experienced temperature gradients in these regions.

The following section evaluates the performance of a solar chimney power plant when combining a slightly modified version of the International Standard Atmosphere (ISA) with the assumed DALR as atmospheric models to the plant. Note that, unless stated otherwise, all references in this paper to the "ISA" refer to the mentioned modified version of the ISA.

4.1 Assumptions by the numerical model

In the analysis of this section, the numerical model makes two assumptions:

- The DALR and ISA should predict a similar atmospheric temperature and pressure at the intersection point of the two lapse rates.
- The higher ambient temperature predicted at any height (by either the DALR or ISA) is always employed as the atmospheric temperature at that height.

4.2 Implementation into the numerical model

According to Kröger[16], the standard ISA for temperate latitudes is a time-independent temperature lapse rate having a mean sea level pressure of 101325 N/m^2, corresponding temperature of 288.15 K and a temperature gradient of 0.0065 K/m. In light of the fact that the reference location (Sishen, South Africa) is situated in a slightly warmer climate, the modified version of the standard ISA is approximated to be a time-independent lapse rate having a mean sea level pressure of 101325 N/m^2, corresponding temperature of 290.65 K and a temperature gradient of 0.0065 K/m. Figure 6 illustrates this modified linear ISA temperature line.

The following modified versions of the equations by Kröger[16] present the temperature and pressure variation with height above sea level (according to the ISA).

$$T = T_{sl} - \frac{dT}{dz} z_{sl} = 290.65 - 0.0065\, z_{sl} \tag{2}$$

$$p = p_{sl}\left[1 - 0.0065\left(\frac{z_{sl}}{T_{sl}}\right)\right]^{5.255} = 101325\left[1 - 0.0065\left(\frac{z_{sl}}{290.65}\right)\right]^{5.255} \tag{3}$$

where T_{sl} and p_{sl} refer to the temperature and pressure at sea level respectively, while z_{sl} is the height above sea level. It should be noted that the reference site (Sishen, South Africa) is located at 1187 m above sea level.

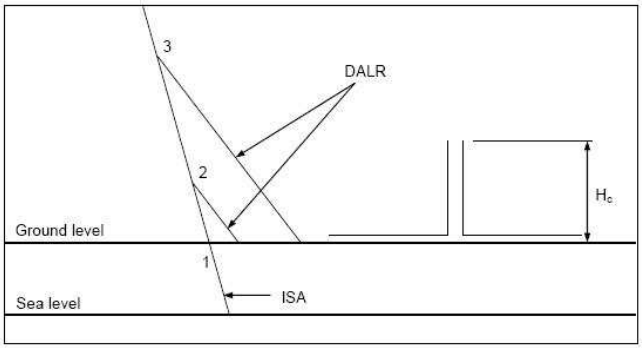

Figure 6: Illustration of the modified ISA (equation 2) and DALR (equation 4) and their implementation into the numerical model

Figure 6 depicts the linear DALR temperature line at two different positions, which represents the DALR for two different times of the day and year. Kröger[16] also presents the following equations for the DALR.

$$T = T_a - \frac{dT}{dz} z = T_a - 0.00975\, z \tag{4}$$

$$p = p_a\left[1 - 0.00975\left(\frac{z}{T_a}\right)\right]^{3.5} \tag{5}$$

where T_a and p_a are the respective ambient temperature and pressure near ground level, while z is the altitude above ground level.

It should be mentioned that experimental daytime temperature measurements by Kröger[16] reveal that, due to a non-linear temperature distribution within a few meters (10 m to 20 m) above ground level, actual ambient air temperatures may effectively be between 1 °C and 2 °C lower than those measured near ground level (1 m to 2 m) and thus predicted by the specified DALR of equation 4. This is illustrated clearly by figure 7. The figure shows the DALR according to equation 4, where T_a is the ambient temperature value near ground level. The actual atmospheric temperature distribution is also indicated, showing the non-linear region near ground level, followed (at a height in the order of 10 m above ground level) by a temperature gradient equal to the specified DALR.

These actual lower atmospheric temperatures would mean a greater driving potential and subsequent greater power output for the solar chimney power plant. For the specified reference plant in the appendix, a lower ambient air temperature of 1 °C over the chimney height results in an annual power output increase in the order of 10 %. This suggests that the current numerical model predicts a conservative yield.

Since the temperature gradients of the DALR and ISA differ, the profiles will intersect at a specific height, depending on the time of day and day of the year. Consider the first assumption of this section. The main implication of this assumption is that the ambient pressure employed at ground level will vary with time, which is in contrast with the constant ambient pressure assumption (p_a = 90000 N/m^2 in the reference plant specification of the appendix). The intersection height above ground level of the two lapse rates is determined by equating equation 2 and equation 4 (since the atmospheric temperature is assumed equal at the intersection point) and simplifying

$$z_{\text{int}} = \frac{\left(T_a - 282.9345\right)}{0.00325} \tag{6}$$

where $z_{sl} = z + 1187$ in equation 2. The atmospheric pressure at the intersection height may then be determined by

$$p_{\text{int}} = 101325\left[1 - 0.0065\left(\frac{z_{\text{int}} + 1187}{290.65}\right)\right]^{5.255} \tag{7}$$

according to the ISA.

Consider the second assumption of this section. This assumption produces a conservative solution. Therefore, if the calculated intersection point is above ground level (e.g. positions 2 and 3 in figure 6) then the ambient pressure at ground level is given by

$$p_a = \frac{p_{\text{int}}}{\left[1 - 0.00975\left(z_{\text{int}}/T_a\right)\right]^{3.5}} \tag{8}$$

as predicted by the DALR. However, if the intersection point is below ground level (e.g. position 1 in figure 6) the ambient pressure at ground level is

$$p_a = 101325\left[1 - 0.0065\left(\frac{1187}{290.65}\right)\right]^{5.255} \tag{9}$$

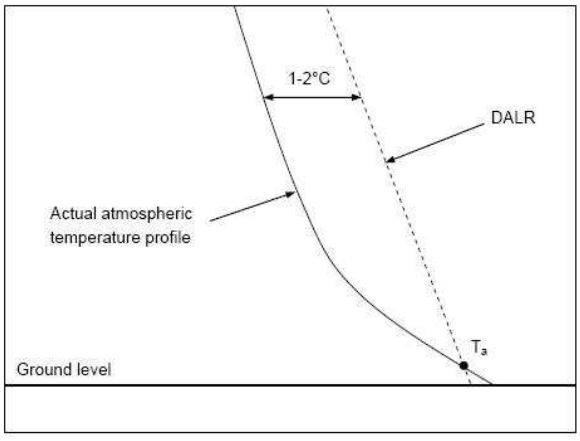

Figure 7: The specified DALR and actual atmospheric temperature distribution

as predicted by the ISA. In addition to determining the ambient pressure at ground level, the temperature and pressure at the height of the chimney outlet must also be determined in order to calculate the Froude number and driving potential of the plant. Once again the second assumption is used by employing the higher temperature predicted by either the DALR or ISA at the chimney outlet height. Consequently, if the intersection height is higher than the chimney height (position 3 in figure 6), the atmospheric temperature and pressure at the chimney outlet height is determined by equation 4 and equation 5 respectively (by substituting the chimney height H_c for z). However, if the calculated intersection height is lower than the chimney height (position 2 in figure 6), the ambient temperature and pressure at the chimney outlet height is given by equation 2 and equation 3 (by substituting H_c + 1187 for z_{sl}).

4.3 Simulation and results

Comparative simulations were conducted for the reference solar chimney power plant with one model employing a combination of the DALR and ISA (according to the strategy mentioned above) while the other model uses only the DALR to model the atmosphere surrounding the solar chimney power plant. Both models employ the DALR inside the chimney of the plant.

Figure 8 indicates a slightly reduced peak power output during the summer months when introducing the DALR / ISA combination atmospheric model. This trend is due to the somewhat reduced (and varying) ambient pressure employed by the DALR / ISA combination model in comparison to the assumption of a constant ground level ambient pressure of p_a = 90000 N/m^2 employed by the DALR model.

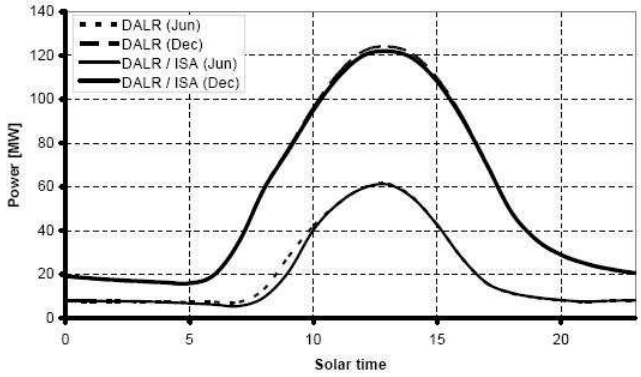

Figure 8: The effect of two atmospheric lapse rate models on daily power output

Another noticeable trend is a decreased power output during most of the morning of the winter months when employing the DALR / ISA combination model. This occurrence is caused by the fact that the DALR / ISA combination model always employs the higher ambient temperature predicted by either the DALR or ISA at any height. During these winter morning periods, the ISA predicts higher ambient temperatures at the chimney outlet height than the DALR and is therefore used by the numerical model. The higher temperatures predicted over the height of the chimney causes a lower driving potential which ultimately results in a lower power output.

Annually, table 3 shows a marginally reduced power output of 0.9 % when incorporating the DALR / ISA combination model in comparison with the DALR atmospheric model.

Plant configuration	Annual power output [GWh]
Dry adiabatic lapse rate (DALR)	336
DALR / ISA combination	333.1

Table 3: Effect of employing a DALR only versus DALR / ISA combination on annual power output

5. Nocturnal Temperature Inversion Effects

The air near the surface of the earth experiences significant daily temperature variations as a result of radiative heating and cooling of the earth's surface. The previous section has mentioned the linear temperature gradients (DALR and ISA) which exist in the atmosphere (figure 6). Under certain conditions, it is possible that temperature inversions may occur in the atmosphere above ground level, as a result of rapid surface cooling.

Normally, in the time just after sunset, the earth's surface cools down rapidly through radiation. This may cause the ground surface to have a lower temperature than the lowest parts of the atmosphere above ground level, which in turn produces a heat flux from these parts of the atmosphere to the ground. This process initiates the formation of a stable layer of air above the ground surface. With sunrise, the ground surface is reheated and the DALR is reinstated in the atmosphere. Certain geographical regions may also experience stronger temperature inversions than others. Strong inversions have been observed in arid and desert areas where solar chimney power plants are most likely to be located.

The following section evaluates the performance of a solar chimney power plant by combining the DALR and ISA as atmospheric models, while also considering inversion effects during the night-time operation of the plant. During the daytime, the numerical model approximates the atmosphere surrounding the solar chimney power plant according to the analysis of the previous section. During the night-time however, this analysis is modified.

5.1 Assumptions by the numerical model

In the analysis of this section, the numerical model makes three assumptions:

- The nocturnal DALR (equation 12) and ISA should predict a similar atmospheric temperature and pressure at the intersection point of the two lapse rates.
- The temperature inversion profile (equation 10) and nocturnal DALR should predict an equal atmospheric temperature and pressure at their intersection point.
- The inversion profile predicts the atmospheric temperature and pressure until it intersects the nocturnal DALR. Thereafter, the nocturnal DALR predicts the ambient conditions until intersecting the modified ISA. After this point, the ISA predicts the atmospheric conditions.

5.2 Implementation into the numerical model

Kloppers[17] presents the following approximate temperature inversion profile during night-time

$$T = T_{ref}\left(\frac{z}{z_{ref}}\right)^{b} \tag{10}$$

where T_{ref} refers to a reference air temperature (in Kelvin) measured at a reference height z_{ref}, which is approximately 1 m above ground level. Thus with z_{ref} = 1 m, T_{ref} may be referred to as T_a. The exponent b is given by

$$b = 0.0035\sin\left(0.0177\,n_d - 2.32392\right) + 0.0065 \tag{11}$$

where n_d is the number of the day of the year. Equation 11 is applicable to a fully developed inversion at a particular location and was developed by fitting it to measured nocturnal temperature data. It should be noted that b actually changes as the temperature inversion develops. These changes are neglected in this analysis.

Kloppers[17] also suggests that the nocturnal temperature distribution above the inversion gradient may be approximated by

$$T = T_{a,\max} - 0.00975\,z - 0.43t \tag{12}$$

where $T_{a,max}$ is the maximum daily ambient temperature at approximately 1 m above ground level, z is the height above ground level and t is the time after sunset, in hours.

Figure 9 illustrates the modified linear ISA profile (equation 2) as well as the inversion (equation 10) and nocturnal DALR (equation 12) profiles at two different positions representing two different times after sunset. Note that the inversion height grows throughout the night. Although such a condition is not experienced according to the meteorological conditions at the reference site, the dashed line in figure 9 indicates that certain geographical areas may experience much lower night-time ambient temperatures and thus inversion profiles reaching much greater altitudes.

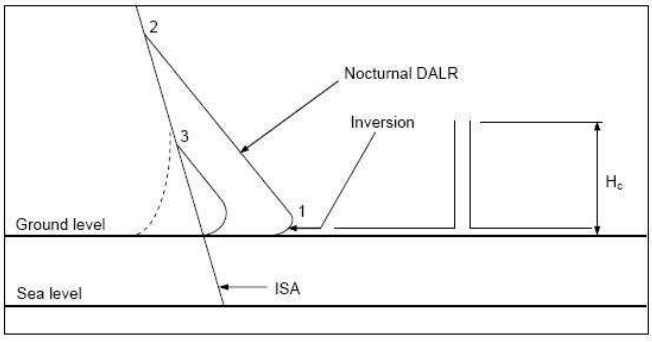

Figure 9: Implementation of modified ISA (equation 2), temperature inversion profile (equation 10) and nocturnal DALR (equation 12)

According to Kröger[16], when assuming the atmospheric air to be a perfect gas, the pressure gradient in a gravity field may be expressed as

$$\frac{dp}{p} = \frac{-g\,dz}{RT} \tag{13}$$

where p and T refer to the respective atmospheric pressure and temperature at any altitude z above ground level, while

g is the gravitational acceleration and R is the specific gas constant. By substituting equation 10 into equation 13 and integrating, we find

$$p = p_a \cdot \exp\left[-\left(\frac{g\, z^{1-b}}{R T_a (1-b)} \right) \right] \tag{14}$$

for the pressure during night-time at any height z above ground level according to the specified temperature inversion profile, where p_a and T_a refer to the ground level ambient pressure and temperature. Similarly, when substituting equation 12 into equation 13 and integrating, we find

$$p = p_a \left[1 - \frac{0.00975\, z}{\left(T_{a,\max} - 0.43t \right)} \right]^{3.5} \tag{15}$$

for the pressure at any height z above ground level according to the nocturnal DALR of Kloppers[17].

Since the temperature gradients of the nocturnal DALR, inversion profile and ISA differ, the profiles will intersect at specific heights, depending on the time of day and day of the year. Consider the first two assumptions of this section. The main implication of these assumptions is that the ambient pressure employed at ground level will vary with time, which is in contrast with the constant ambient pressure assumption (p_a = 90000 N/m^2 in the reference plant specification of the appendix). The intersection height above ground level of the nocturnal DALR and ISA is determined by equating equation 2 and equation 12 (since the atmospheric temperature is assumed equal at the intersection point) and simplifying

$$z_{\text{int}} = \frac{\left(T_{a,\max} - 282.9345 - 0.43t \right)}{0.00325} \tag{16}$$

where $z_{sl} = z + 1187$ in equation 2. The atmospheric pressure at the intersection height (p_{int}) may then be determined according to equation 7. When considering the first assumption of this section, the ambient pressure at ground level as predicted by the nocturnal DALR is

$$p_a = \frac{p_{\text{int}}}{\left[1 - \left(0.00975\, z_{\text{int}} \right) \Big/ \left(T_{a,\max} - 0.43t \right) \right]^{3.5}} \tag{17}$$

The intersection height above ground level of the inversion profile and the nocturnal DALR (e.g. position 1 in figure 9) is determined by equating equation 10 and equation 12 (since the atmospheric temperature is assumed equal at the intersection point) and simplifying

$$T_a\, z^b = T_{a,\max} - 0.00975\, z - 0.43t \tag{18}$$

where the intersection point ($z_{int,2}$) is determined by solving equation 18 iteratively. At this intersection height, the ambient pressure $p_{int,2}$ is determined according to equation 15, where $z_{int,2}$ is substituted into z and p_a is taken from equation 17. When considering the second and third assumption of this section, the ambient pressure as predicted by the inversion profile can be calculated as follows

$$p_a = \left(p_{\text{int},2} \right) \Big/ \exp\left[-\left(\frac{g\, z_{\text{int},2}^{1-b}}{R T_a (1-b)} \right) \right] \tag{19}$$

This pressure is employed as the ambient pressure for the DALR / ISA / Inversion atmospheric model. The temperature and pressure at the height of the chimney outlet must also be determined in order to calculate the Froude number and driving potential of the plant. Once again we consider the third assumption of this section. Consequently, if the intersection height from equation 16 is higher than the chimney height (e.g. position 2 in figure 9), the atmospheric temperature and pressure at the chimney outlet height is determined by equation 12 and equation 15 respectively (by substituting the chimney height H_c for z). However, if the calculated intersection height is lower than the chimney height (e.g. position 3 in figure 9), the ambient temperature and pressure at the chimney outlet height is given by equation 2 and equation 3 (by substituting H_c + 1187 for z_{sl}).

5.3 Simulation and results

Comparative computer simulations were conducted for the reference solar chimney power plant. One model employs a combination of the DALR and ISA during the daytime and a combination of the nocturnal DALR, ISA and inversion profile during the night-time. The other model uses only the DALR to model the atmosphere surrounding the solar chimney power plant. Both models employ the DALR inside the chimney of the plant.

Figure 10 illustrates a considerably lower night-time power output throughout the year for the DALR / ISA / Inversion model compared to the DALR model. This phenomenon can be ascribed to the nocturnal temperature inversions. In effect, such temperature inversions near the ground surface cause higher atmospheric air temperatures over the height of the chimney than predicted by the DALR model. This leads to a reduced driving potential and a subsequently reduced power output.

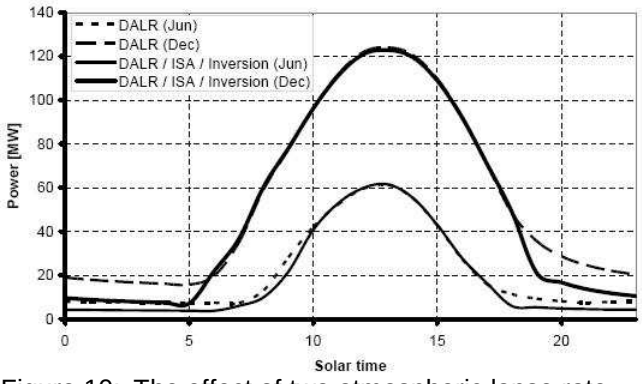

Figure 10: The effect of two atmospheric lapse rate models on daily power output

Analogous to the results of the previous section, figure 10 also indicates a marginally reduced peak power output during the summer months when introducing the DALR / ISA / Inversion combination atmospheric model. This is

due to the somewhat reduced (and varying) ambient pressure employed by the DALR / ISA / Inversion model.

Also similar to the results of the previous section is a decreased power output during most of the morning of the winter months when employing the DALR / ISA / Inversion combination model. This is caused by the fact that the DALR/ISA/Inversion model employs the higher temperature predicted by either the DALR or ISA during these times. During winter mornings, the ISA predicts higher temperatures at the chimney outlet height than the DALR and is therefore employed by the numerical model. The higher temperatures over the height of the chimney causes a lower driving potential which ultimately results in a lower power output.

Table 4 indicates a significantly reduced power output of 7.7 % when incorporating the DALR / ISA / Inversion combination model in comparison with the DALR atmospheric model.

Plant configuration	Annual power output [GWh]
Dry adiabatic lapse rate (DALR)	336
DALR / ISA / Inversion combination	310.1

Table 4: Effect of employing a DALR only versus DALR / ISA / Inversion combination on annual power output

It should be noted that inversion effects at the reference location are relatively weak, yet the effect thereof on the power production of the solar chimney power plant is already measurable. In areas where stronger inversions occur this effect will be correspondingly more pronounced.

6. Conclusion

The effects of wind, ambient temperature lapse rates and nocturnal temperature inversions on plant performance were evaluated. Results show that the prevailing ambient winds at the reference site does have a considerable influence, by reducing annual plant output by approximately 10 %, compared to the same plant experiencing no-wind conditions throughout the year. Moreover, simulations indicate that the existence of nocturnal temperature inversions will also have a significant negative effect on plant performance. The variation of the ambient wind profile and the existence of an International Standard Atmosphere (without nocturnal temperature inversions) in the atmosphere surrounding the solar chimney power plant illustrate minor effects (less than 2.5 %) on annual plant yield.

7. Acknowledgements

We would like to thank the National Research Foundation (NRF) and the Volkswagen Stiftung for their financial support.

References

1. *Haaf W, Friedrich K, Mayr G and Schlaich J*, Solar chimneys, part I: Principle and construction of the pilot plant in Manzanares, *International Journal of Solar Energy*, 1983, 2, 3-20.
2. *Haaf W*, Solar chimneys, part II: Preliminary test results from the Manzanares pilot plant, *International Journal of Solar Energy*, 1984, 2, 141-161.
3. *Schlaich J*, The Solar Chimney: Electricity from the Sun, Deutsche Verlags-Anstalt, Stuttgart, 1994.
4. *Pasumarthi N and Sherif SA*, Experimental and theoretical performance of a demonstration solar chimney model – part I: Mathematical model development, *International Journal of Energy Research*, 1998, 22(3), 277-288.
5. *Pasumarthi N and Sherif SA*, Experimental and theoretical performance of a demonstration solar chimney model – part II: Experimental and theoretical results and economic analysis, *International Journal of Energy Research*, 1998, 22(5), 443-461.
6. *Kröger DG and Buys JD*, Performance evaluation of a solar chimney power plant, *ISES 2001 Solar World Congress*, Adelaide, Australia, 2001.
7. *Gannon AJ and Von Backström TW*, Controlling and maximizing solar chimney power output, *1st International Conference on Heat Transfer, Fluid Mechanics and Thermodynamics HEFAT 2002*, Kruger Park, South Africa, 2002.
8. *Gannon AJ and Von Backström TW*, Solar chimney turbine performance, *Journal of Solar Energy Engineering*, 2003, 125, 101-106.
9. *Bernardes MA dos S, Voβ A and Weinrebe G*, Thermal and technical analyses of solar chimneys, *Solar Energy*, 2003, 75(6), 511-524.
10. *Pastohr H, Kornadt O and Gürlebeck K*, Numerical and analytical calculations of the temperature and flow field in the upwind power plant, *International Journal of Energy Research*, 2004, 28, 495-510.
11. *Pretorius JP, Kröger DG, Buys JD and Von Backström TW*, Solar tower power plant performance characteristics, Proceedings of the *ISES EuroSun2004 International Sonnenforum*, 1, Freiburg, Germany, 2004, PSE GmbH, Freiburg, 870-879.
12. *Serag-Eldin MA*, Computing flow in a solar chimney plant subject to atmospheric winds, Proceedings of *HT-FED04 2004 ASME Heat Transfer / Fluids Engineering Summer Conference*, Charlotte, North Carolina, USA, 2004.
13. *Bilgen E and Rheault J*, Solar chimney power plants for high latitudes, *Solar Energy*, 2005, 79(5), 449-458.
14. *Pretorius JP and Kröger DG*, Solar chimney power plant performance, *Journal of Solar Energy Engineering*, 2006, 128(3), 302-311.
15. *Pretorius JP and Kröger DG*, Sensitivity analysis of the operating and technical specifications of a solar chimney power plant, *Journal of Solar Energy Engineering*, 2007, 129, 171-178.
16. *Kröger DG*, Air-cooled Heat Exchangers and Cooling Towers, Pennwell Corp., Tulsa, Oklahoma, 2004.
17. *Kloppers JC*, A critical evaluation and refinement of the performance prediction of wet-cooling towers, PhD (Eng) thesis, Department of Mechanical and Mechatronic Engineering, University of Stellenbosch, Stellenbosch, South Africa, 2003.

Appendix

A reference solar chimney power plant and typical operating environment is defined by Pretorius and Kröger[14] and its main parameters are repeated here for convenience (see figure 1). The reference site is near Sishen, South Africa, located at latitude 26.67° South and longitude 23.00° East.

Collector roof (Glass)

Emissivity of glass	$e_r = 0.87$
Roughness of glass	$\varepsilon_r = 0$ m
Extinction coefficient of glass	$C_e = 4$ m^{-1}
Refractive index of glass	$n_r = 1.526$
Thickness of glass	$t_r = 0.004$ m
Roof shape exponent	$b = 1$
Perimeter (inlet) height	$H_2 = 5$m
Outer diameter	$d_2 = 5000$ m
Inner diameter	$d_3 = 400$ m
Inlet loss coefficient	$K_i = 1$
Support diameter	$d_s = 0.2$ m
Support drag coefficient	$C_{sD} = 1$
Support tangential pitch	$P_t = 10$ m
Support radial pitch	$P_r = 10$ m

Ground

Type	Sandstone
Emissivity (treated surface)	$e_g = 0.9$
Absorptivity (treated surface)	$\alpha_g = 0.9$
Density	$\rho_g = 2160$ kg/m^3
Specific heat capacity	$c_g = 710$ J/kgK
Thermal conductivity	$k_g = 1.83$ W/mK
Roughness	$\varepsilon_g = 0.05$ m

Chimney (Concrete)

Height	$H_c = 1000$ m
Inside diameter	$d_c = 210$ m
Bracing wheel (one) drag coefficient	$K_{bw} = 0.01$
Number of bracing wheels	$n_{bw} = 10$
Inside wall roughness	$\varepsilon_c = 0.002$ m

Turbine

Turbo-generator efficiency	$\eta_{tg} = 80$ %
Inlet loss coefficient	$K_{turb,i} = 0.14$

Ambient conditions

Atmospheric pressure	$p_a = 90000$ N/m^2